Constraints on Enhanced Weathering and related carbon sequestration – a cropland mesocosm approach

Amann, Thorben; Hartmann, Jens; Struyf, Eric; de Oliveira Garcia, Wagner; Fischer, Elke Kerstin;

Janssens, Ivan; Meire Patrick; Schoelynck, Jonas

Supplementary material

S1. Soil and rock characterization

The soil was provided by the *Bodemkundige Dienst van België* in 2013. Initial soil pH was reported as 7.8. The bulk density was 1.15 g cm^{-3} (dry mass) at a soil moisture of 16%.

Basic granulometric data for the soil amended with rock powder and the rock powder alone can be found in Figs. S1 and S2, respectively.

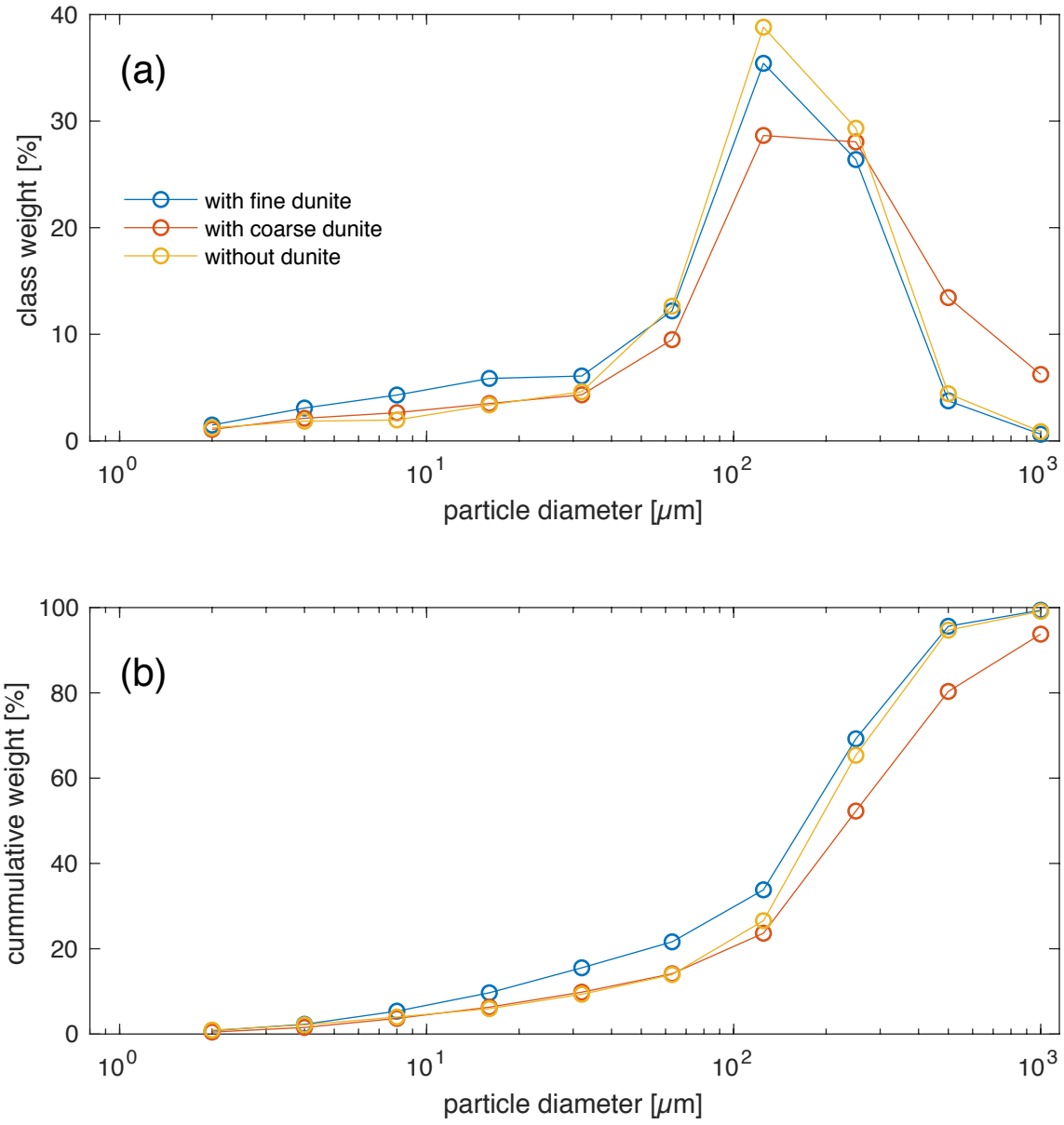

Fig. S1. *Granulometric analyses of the topsoil with and without amended dunite material of fine and coarse grain size.*

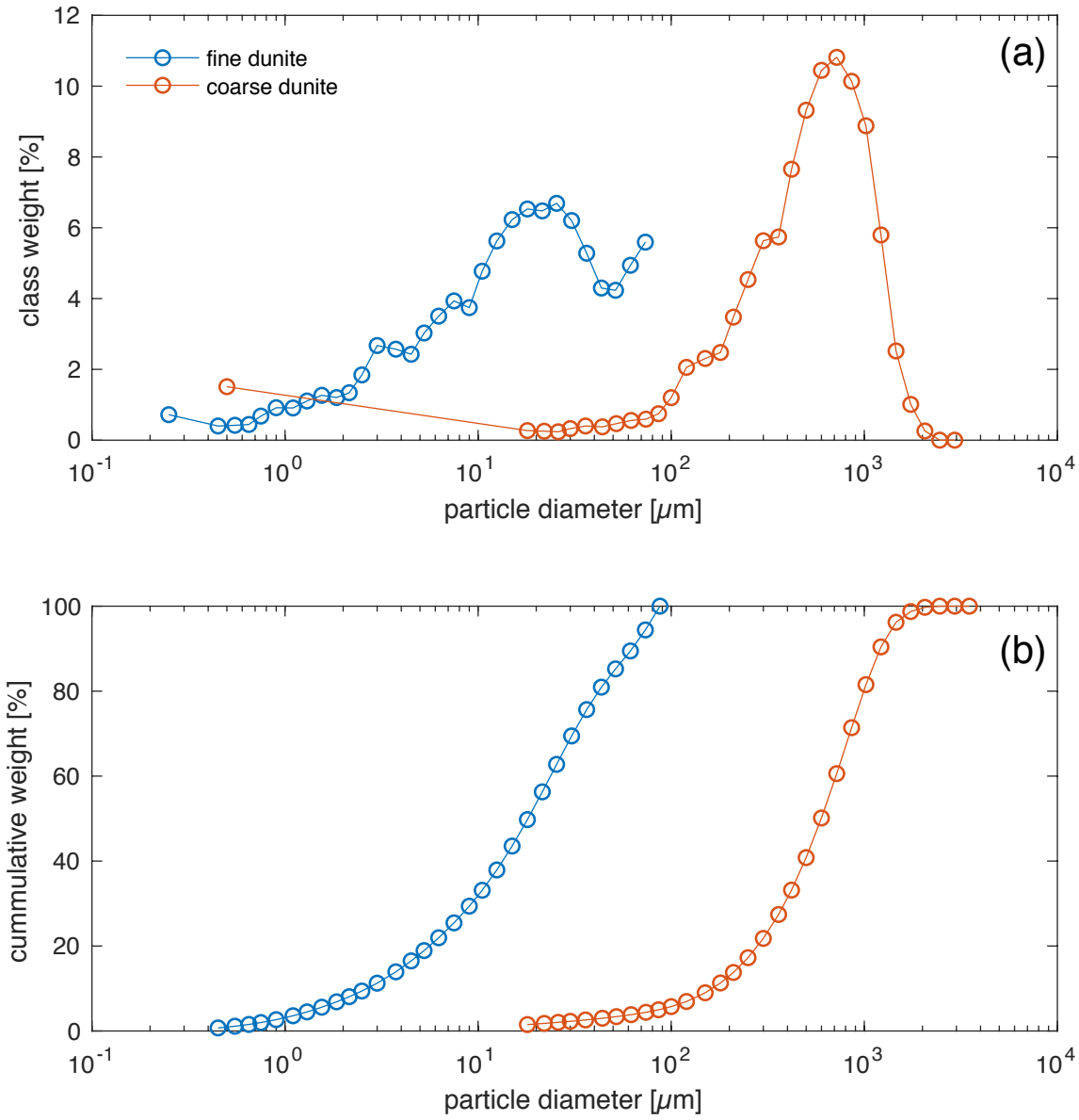

Fig. S2. *Granulometric analyses of the dunite material used. (a) shows the class weight distribution and (b) the cumulative class weight.*

S2. DIC concentrations

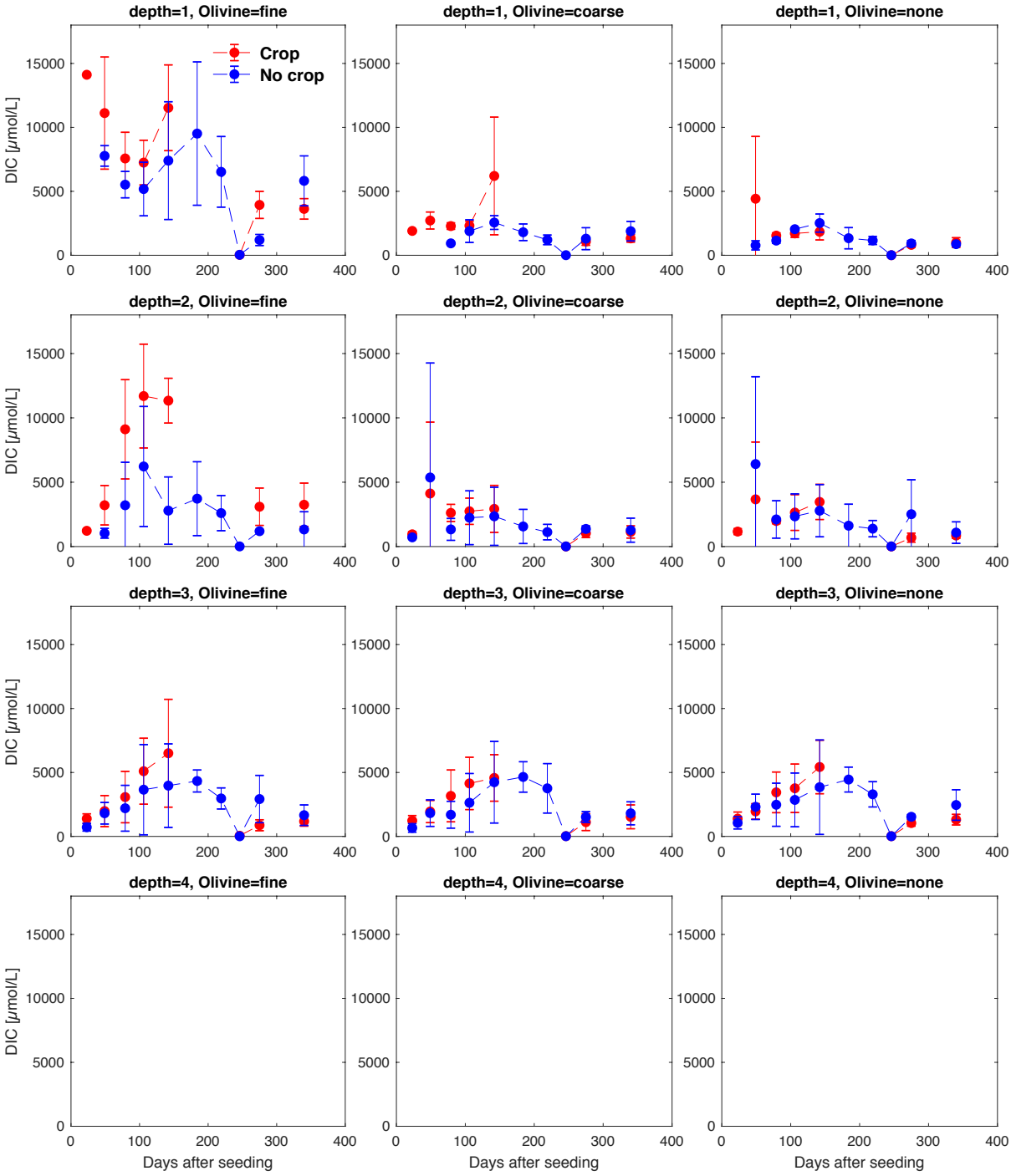

Fig. S3. *Development of DIC concentrations over one year where available, differentiated by olivine and crop treatment. Error bars indicate ±1SD.*

S3. pH

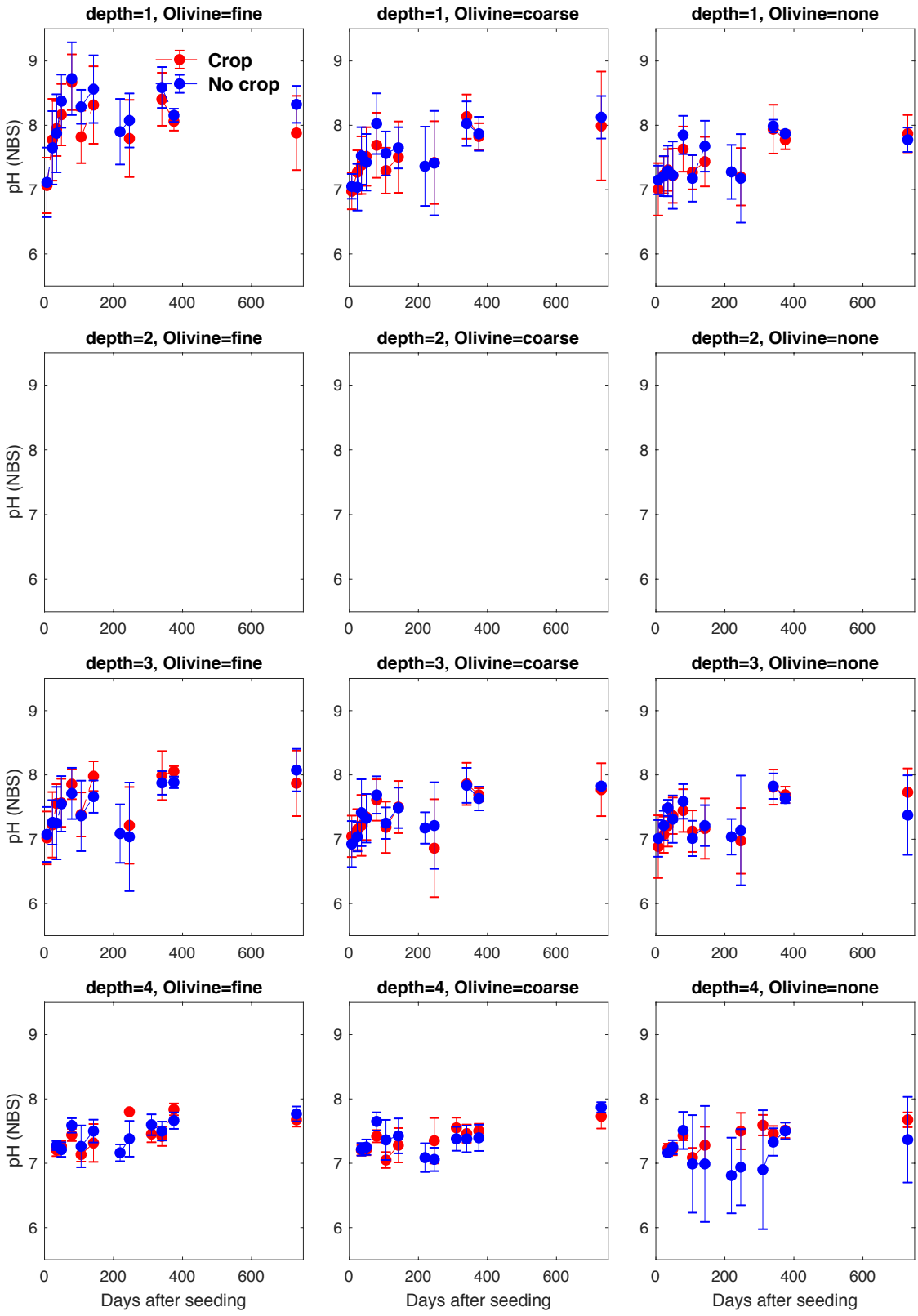

Fig. S4. *Development of pH over the experiment time, differentiated by olivine and crop treatment. Error bars indicate ±1SD.*

S4. Mg concentrations

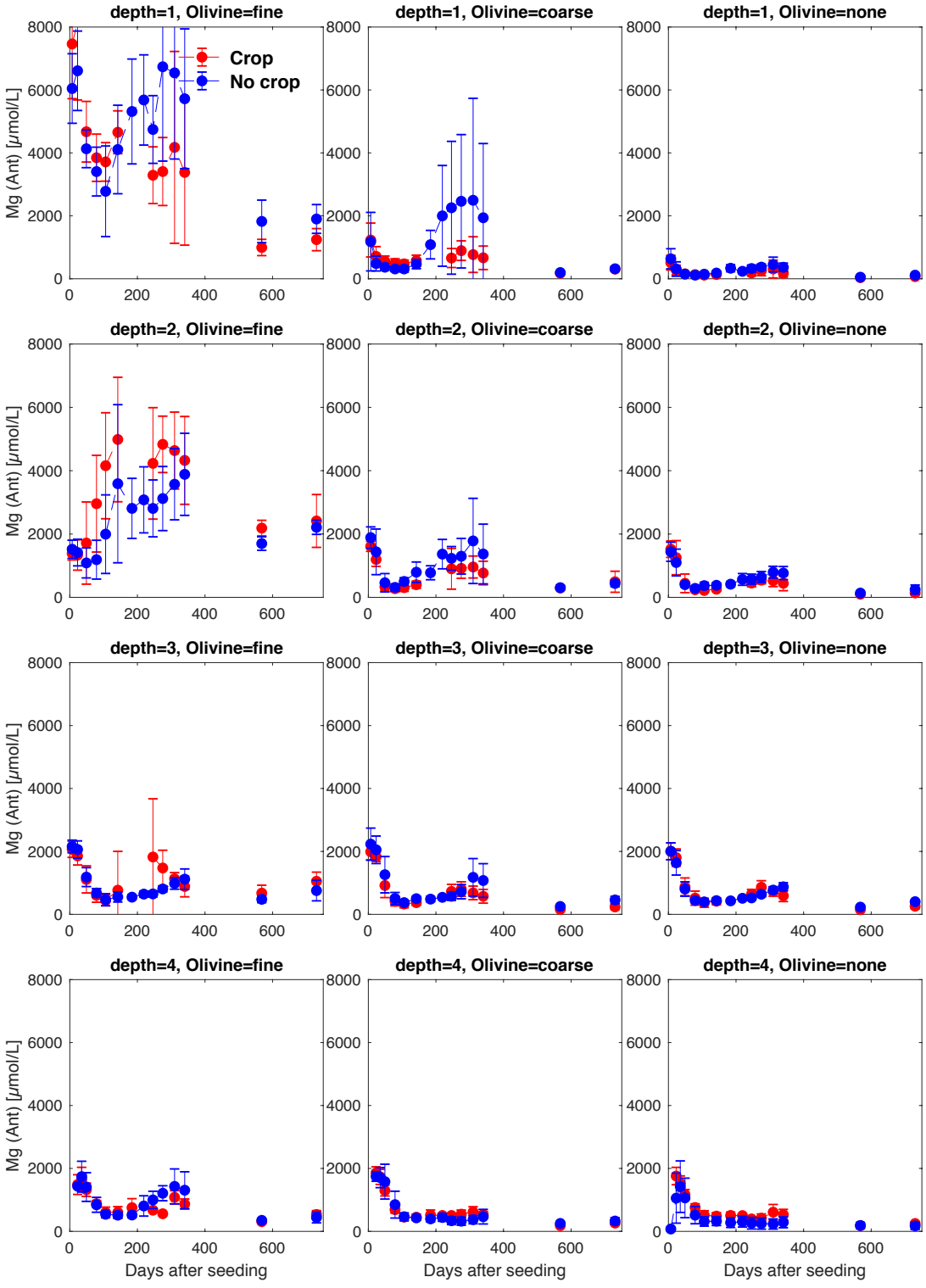

Fig. S5. *Development of Mg concentrations over the experiment time, differentiated by olivine and crop treatment. Error bars indicate ±1SD.*

S5. DSi concentrations

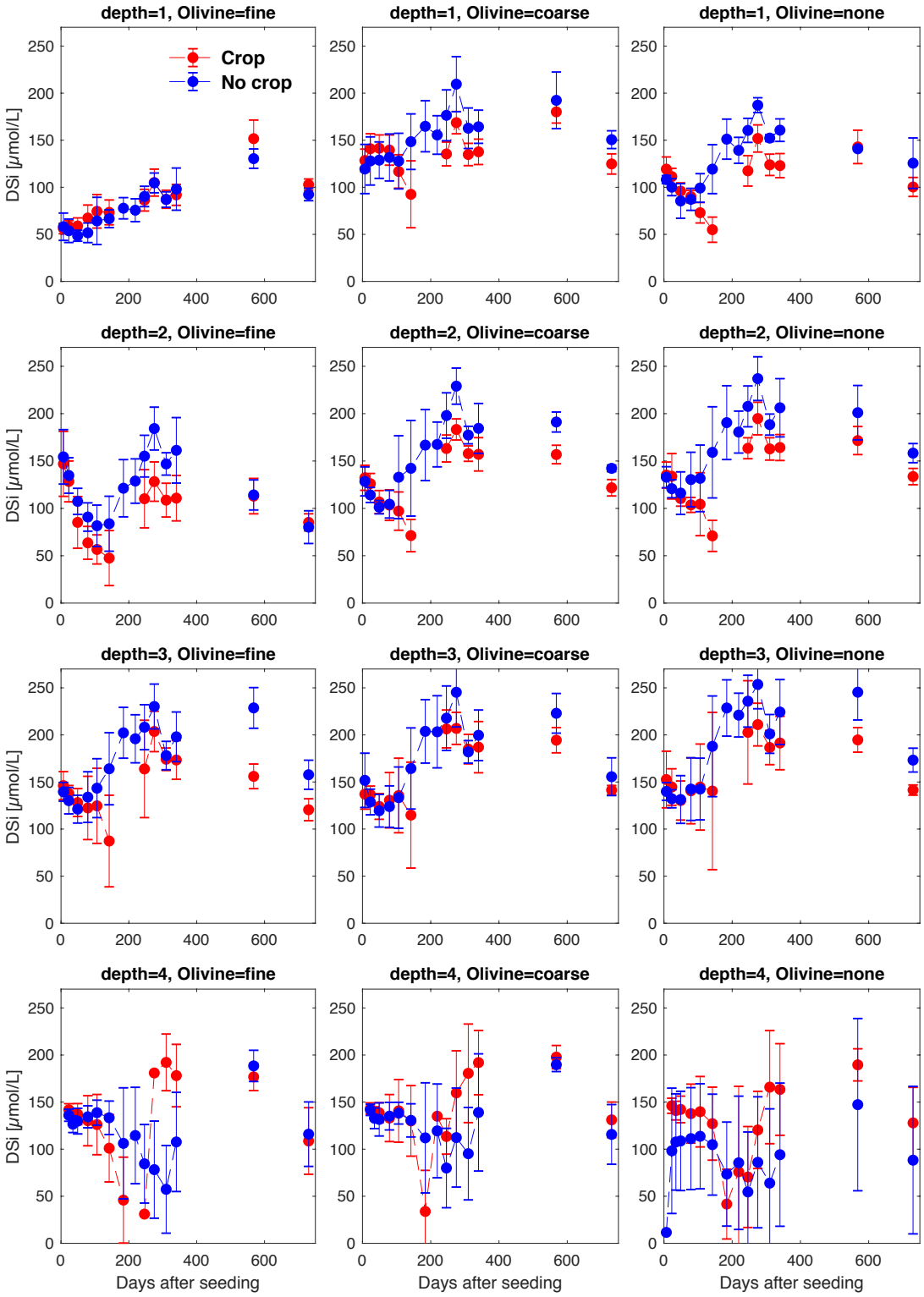

Fig. S6. *Development of DSi concentrations over the experiment time, differentiated by olivine and crop treatment. Error bars indicate ±1SD.*

S6. Mg/Si ratios

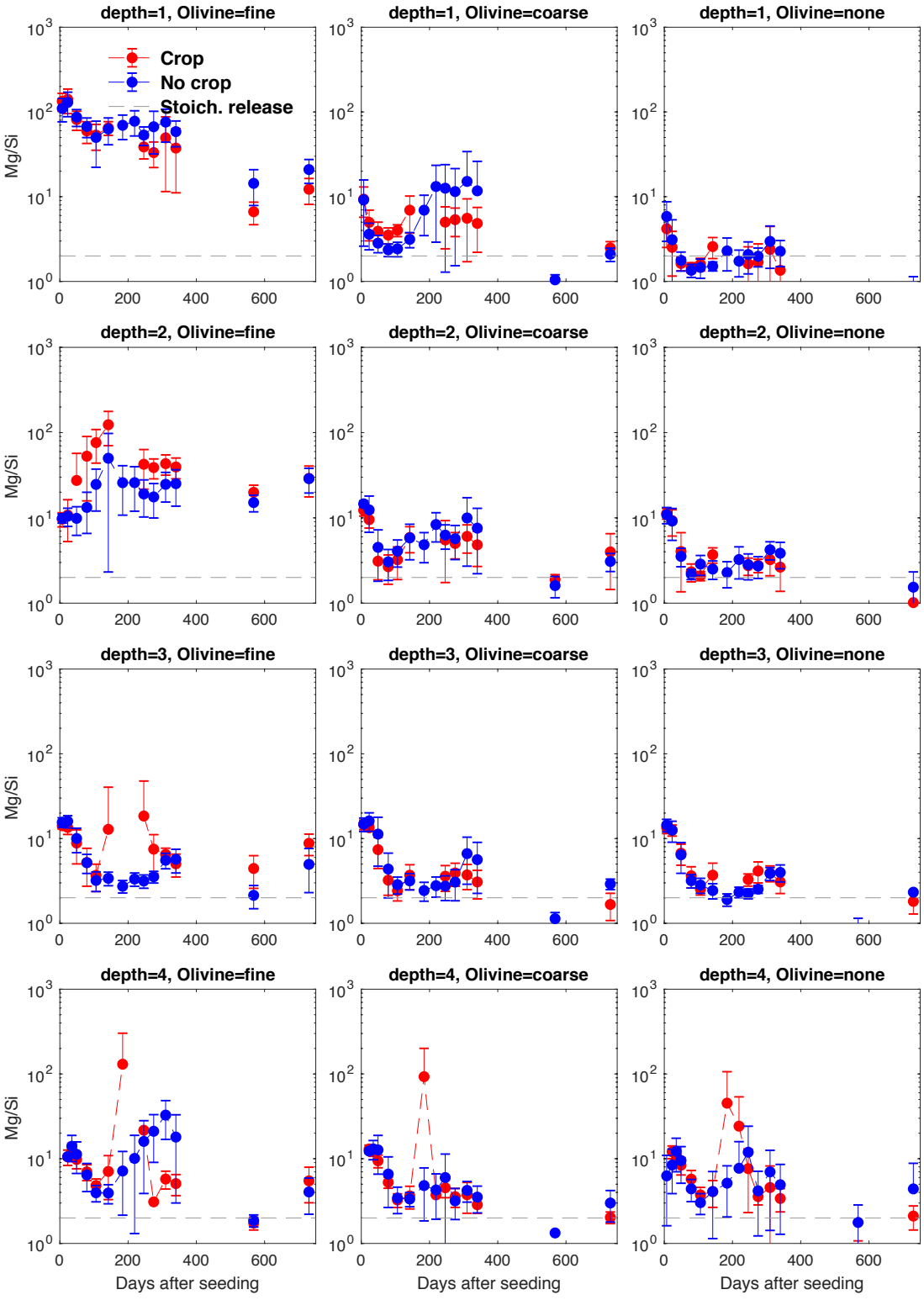

Fig. S7. *Development of Mg/Si ratios over the experiment time, differentiated by olivine and crop treatment. Error bars indicate ±1SD.*

S7. Cr concentrations

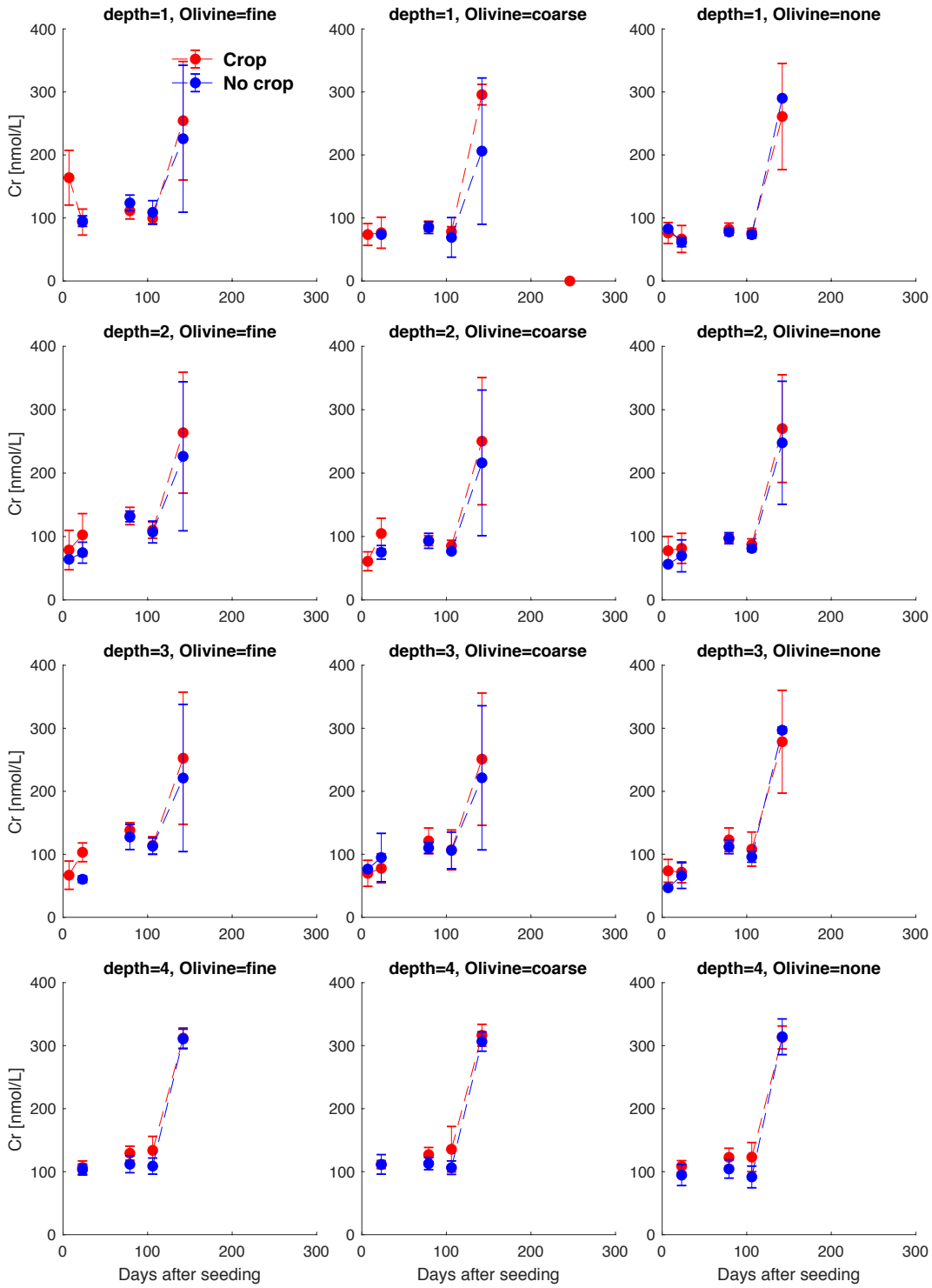

Fig. S8. *Development of Cr concentrations over the experiment time, differentiated by olivine and crop treatment. Error bars indicate ±1SD.*

S8. Ni concentrations

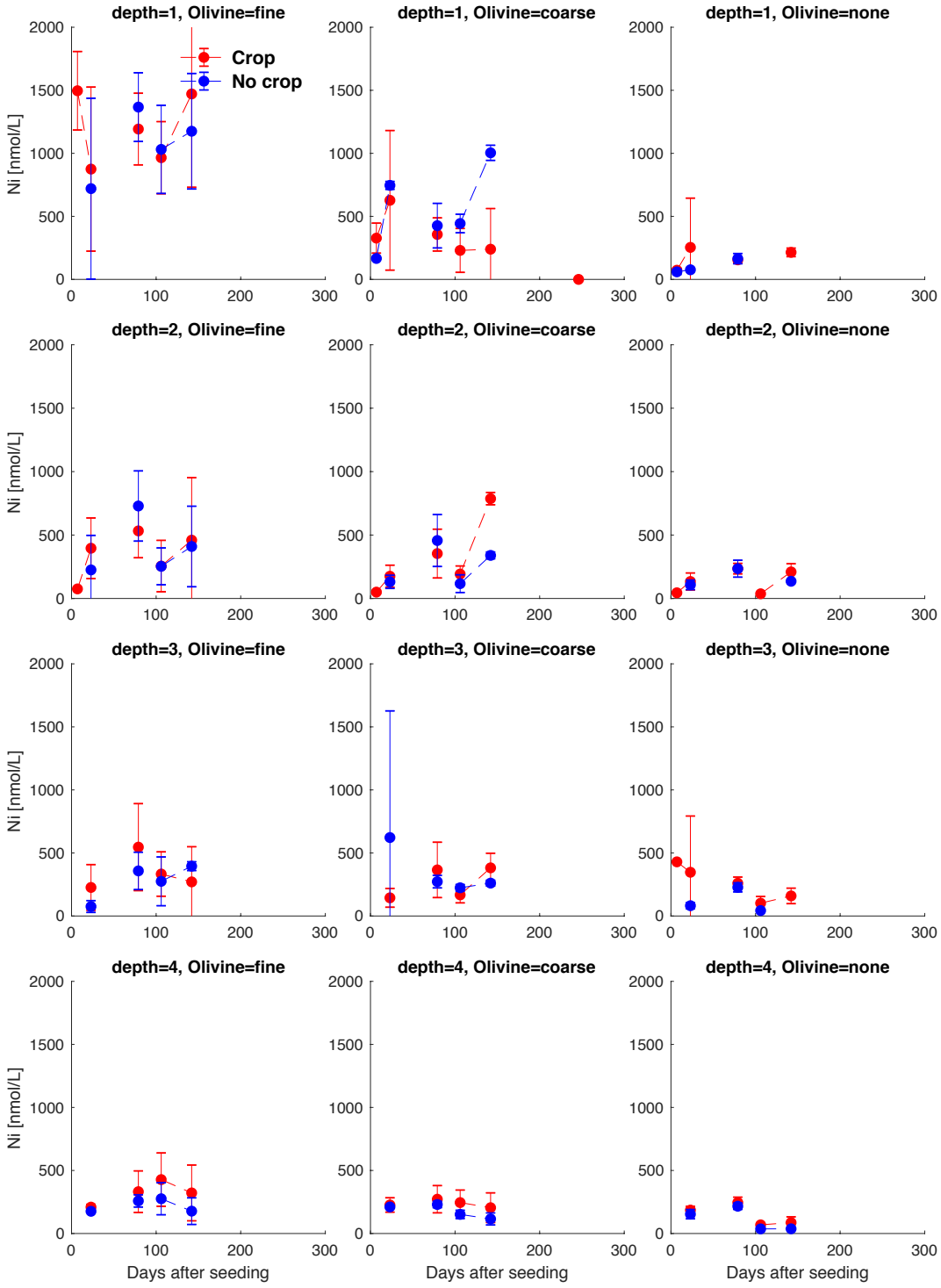

Fig. S9. *Development of Ni concentrations over the experiment time, differentiated by olivine and crop treatment. Error bars indicate ±1SD.*

S9. Trace element accumulation in the topsoil

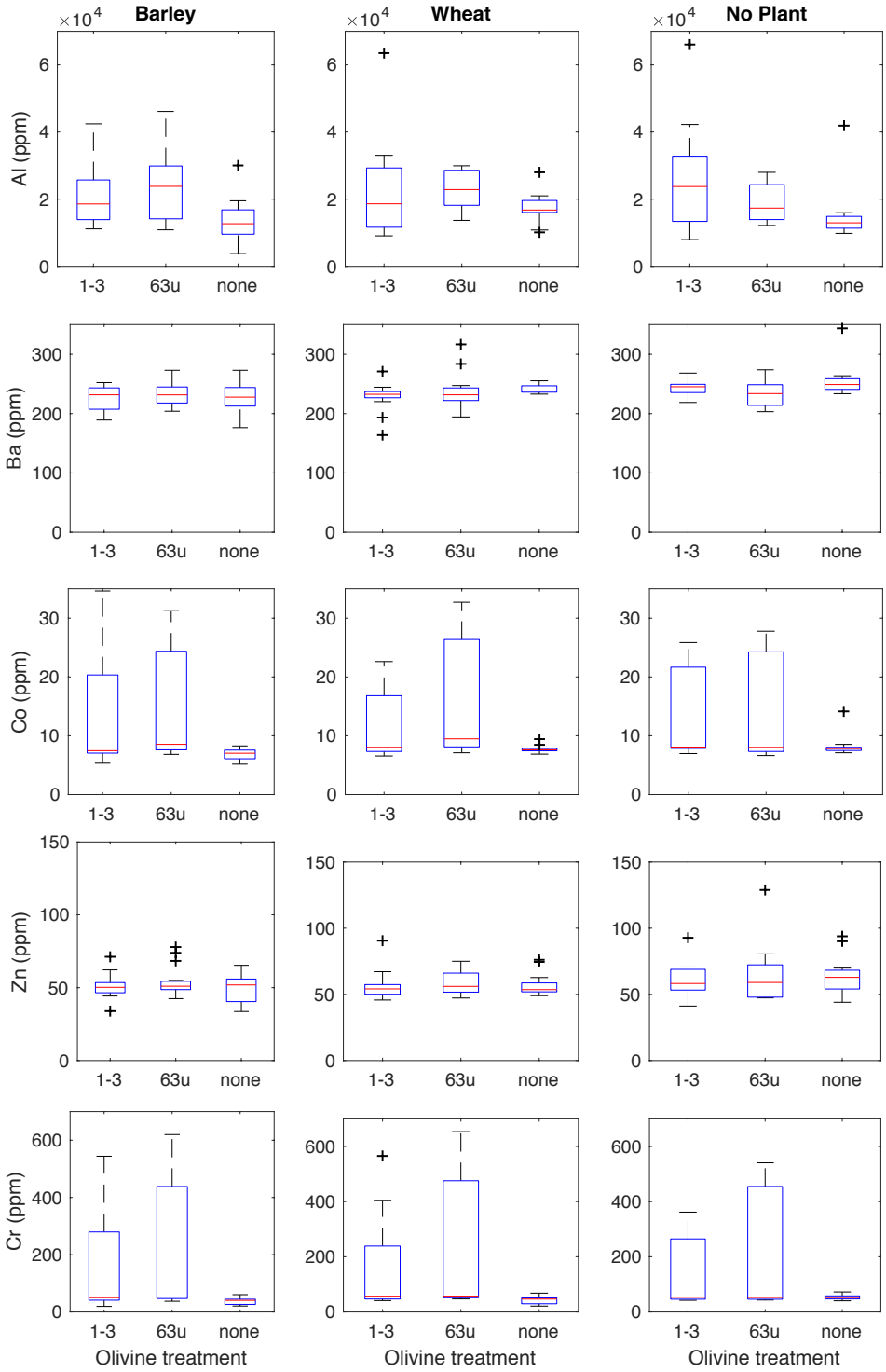

Fig. S10. *Trace metal concentrations in the topsoil. Part 1*

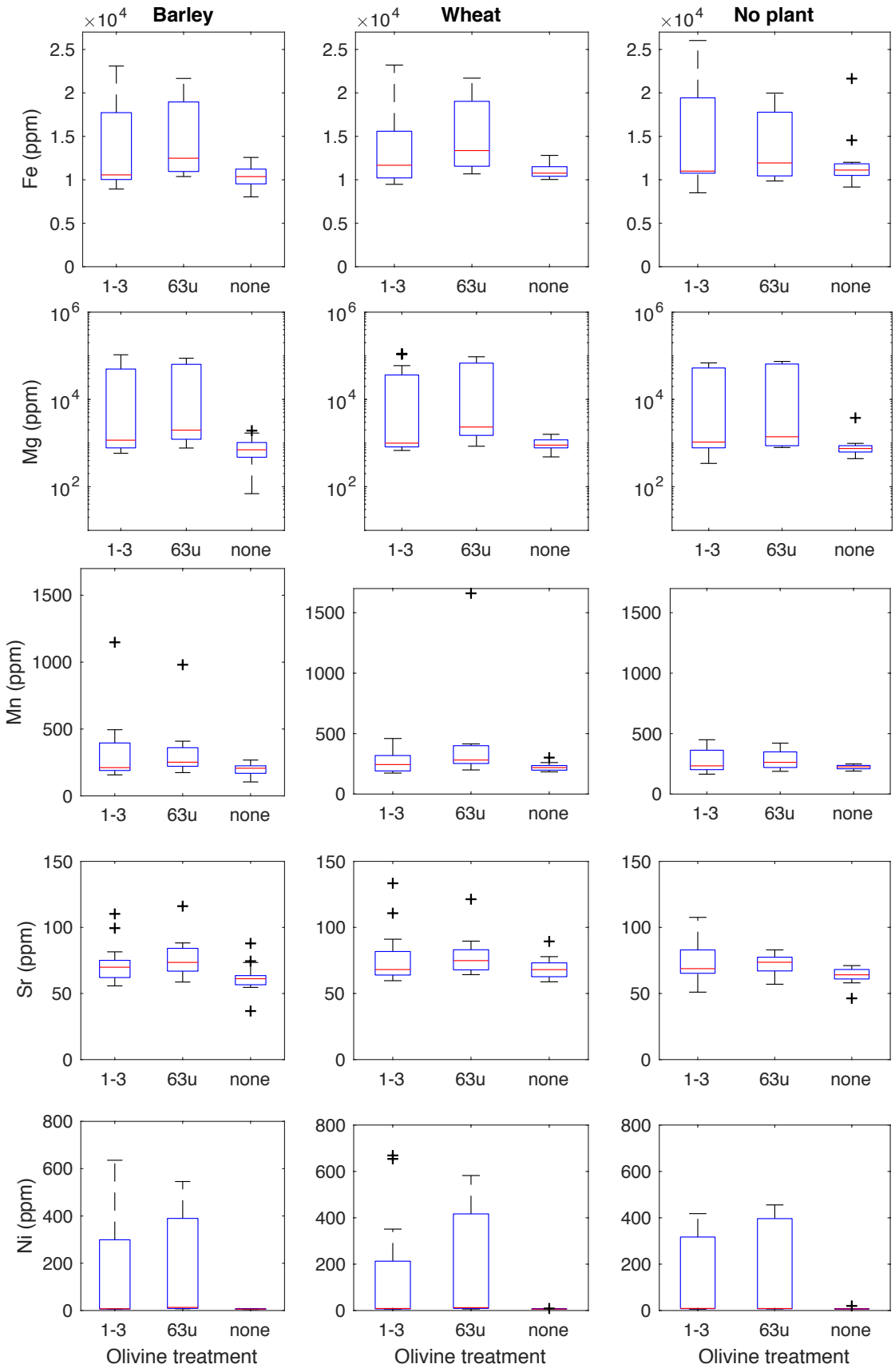

Fig. S11. *Trace metal concentrations in the topsoil. Part 2*

S10. Mg fluxes from the outlet

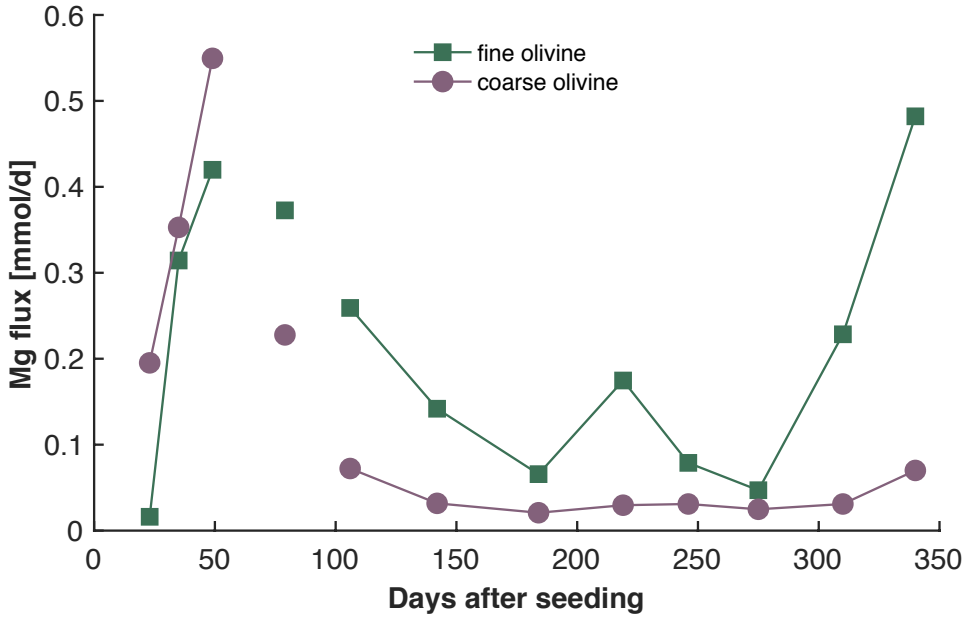

Fig. S12. *Fluxes of Mg from the outlet, corrected for background Mg release (no treatment values). Values refer to the daily-normalised flux of the interval preceding the sampling day.*

S11. Partial pressure of CO_2 in the soils

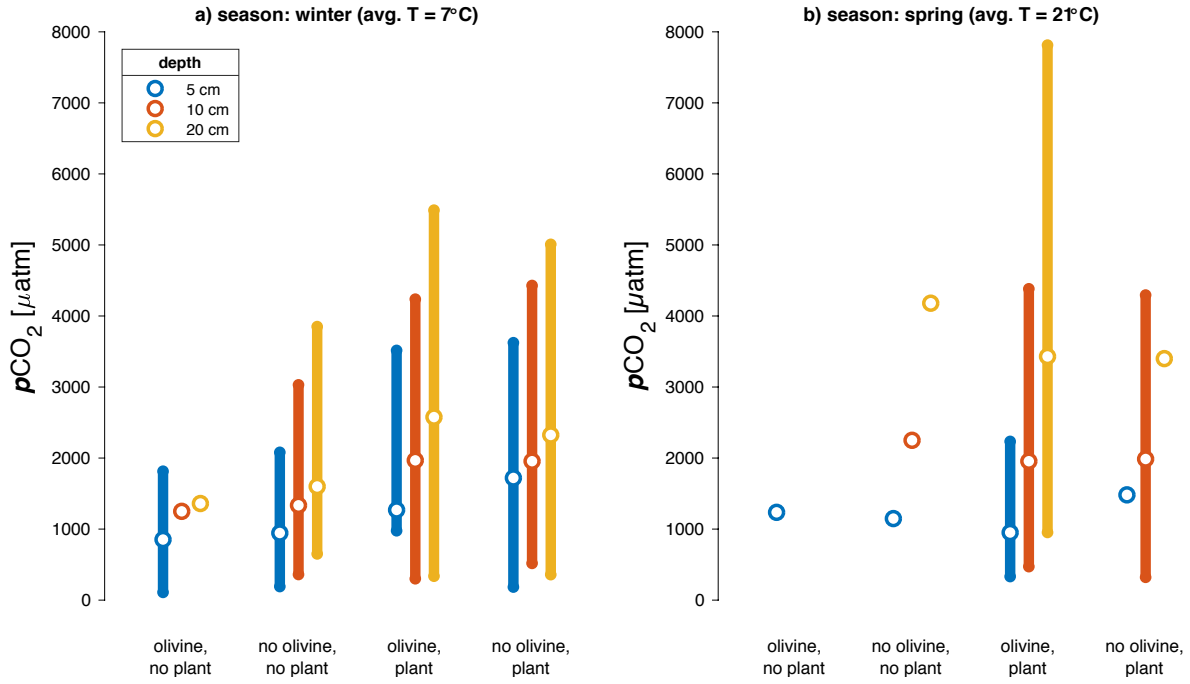

Fig. S13. Partial pressure of CO_2 (pCO_2) measured in selected mesocosms at different depth in winter (a) and spring (b). Bars indicate ±1 SD.

S12. pH development over time

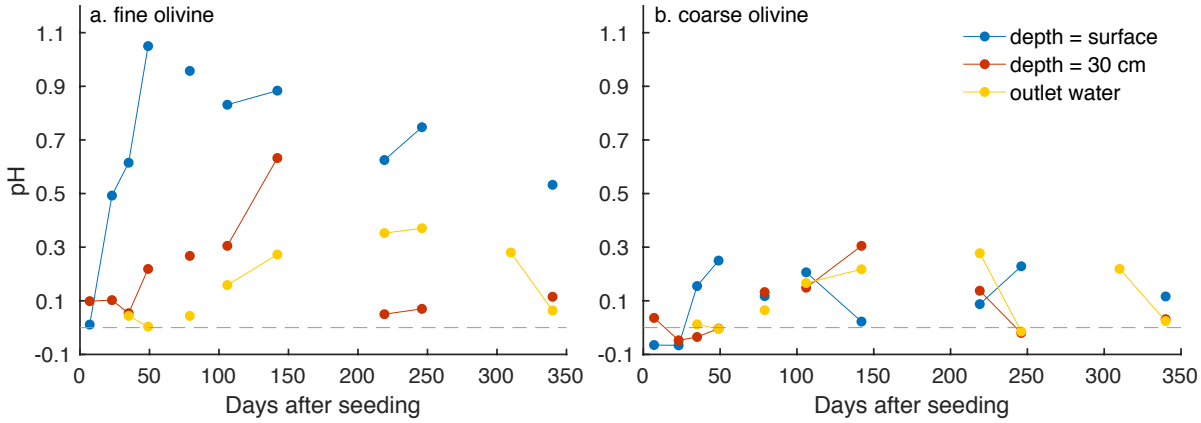

Fig. S14. *Mean pH anomaly in the soil pore water of olivine treated mesocosms (with increasing depths) throughout the experiment time, relative to the control (pore water w/o olivine treatment, and irrigation water, dashed line: blank). Differences in pH were calculated with pH values and do thereby not directly represent proton concentration differences.*

S13. Ni and Cr concentrations corrected for blank values

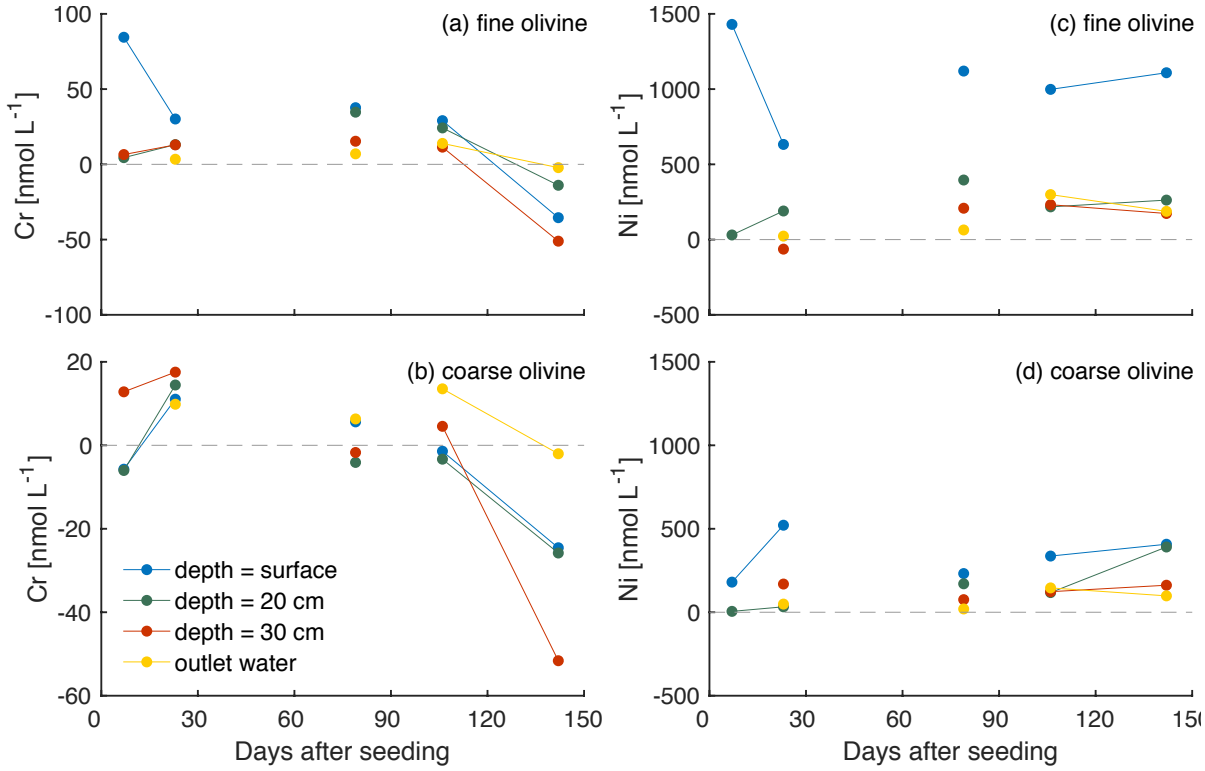

Fig. S15. Average concentrations of Cr (a) and Ni (b) relative to the control (pore water w/o olivine treatment) in the soil pore water of olivine treated mesocosms over the first 5 months, relative to the control (pore water w/o olivine treatment).

S14. Calculation of weathering and CO_2 sequestration rates

The average flux of Mg from dunite amended soils at the outlet can be calculated by

$$Flux_{Mg^{2+}} = ([Mg^{2+}]_{treated} - [Mg^{2+}]_{untreated}) \times q \qquad \textit{Eq. S1}$$

With *q* as water volume discharged at the outlet per sampled time interval.

The sequestration rate can subsequently be calculated by

$$CO_2\ sequestration = \frac{Flux_{Mg^{2+}} \times molweight_{Mg}}{fraction\ of\ Mg\ in\ Forsterite} \times RCO_2 \qquad \textit{Eq. S2}$$

with a RCO2 of 1.1 as claimed by Hartmann et al. (2013).

The global CO_2 sequestration potential was then calculated by multiplying with the available arable land in an optimistic and a pessimistic scenario (Moosdorf et al., 2014).

The weathering rate can be estimated by

$$Weathering\ rate\ R\ \left[\frac{mol\ Olivine}{m^2 s}\right] = \frac{\frac{Flux_{Mg^{2+}}}{2}}{applied\ mass_{olivine} \times specific\ surface\ area \times t} \qquad \textit{Eq. S3}$$

The numerator converts the molar flux of Mg to molar flux of olivine (2 mol Mg per 1 mol olivine). Time factor *t* is used to convert the flux measured in 340 days to seconds.

S15. Calculation of the amorphous Si layer

The Mg depleted and Si enriched layer that forms during the dissolution process (Daval et al., 2011) was roughly estimated using the release of Mg in conjunction with the Mg/Si ratio and the available surface area of the forsterite:

The mass of SiO_2that precipitated per year as amorphous Si can be estimated by

$$m_{SiO_{2amorph.}}\left[\frac{g\ SiO_2}{a}\right] = \left(\frac{R_{Mg}}{Mg/Si_{theoretical}} - R_{Si}\right) \times M_{SiO_2} \times\ t \qquad \textit{Eq. S4}$$

with the dissolution (weathering) rates R_{Mg}, R_{Si}, calculated from experimental data, the theoretical Mg/Si ratio (1.7), M_{SiO2} as the molar mass of SiO_2, and time factor *t* to convert seconds to years.

The depletion layer thickness can then be calculated as

$$growth\ rate\ of\ SiO_2\ layer\ \left[\frac{nm}{a}\right] = \frac{m_{SiO_{2amorph.}}}{\rho_{SiO_{2amorph.}} \times \left(1 - \varphi_{SiO_{2amorph.}}\right)} \times 10^9 \qquad \textit{Eq. S5}$$

with the density $\rho_{SiO2amorph}$ as 2.23 x 10^6 g m^{-3} (Iler, 1979) with the porosity $\varphi_{SiO2amorph}$ as 0.3 (20-40 %; Maher et al., 2016).

S16. References

Daval, D., Sissmann, O., Menguy, N., Saldi, G. D., Guyot, F., Martinez, I., Corvisier, J., Garcia, B., Machouk, I., Knauss, K. G., and Hellmann, R.: Influence of amorphous silica layer formation on the dissolution rate of olivine at 90 °C and elevated pCO2, Chemical Geology, 284, 193-209, http://dx.doi.org/10.1016/j.chemgeo.2011.02.021, 2011.

Hartmann, J., West, A. J., Renforth, P., Köhler, P., De La Rocha, C. L., Wolf-Gladrow, D. A., Dürr, H. H., and Scheffran, J.: Enhanced chemical weathering as a geoengineering strategy to reduce atmospheric carbon dioxide, supply nutrients, and mitigate ocean acidification, Rev Geophys, 51, 113-149, 10.1002/Rog.20004, 2013.

Iler, R. K.: The Chemistry of Silica. Solubility, Polymerization, Colloid and Surface Properties, and Biochemistry, John Wiley & Sons, New York/Chichester/Brisbane/Toronto, 866 pp., 1979.

Maher, K., Johnson, N. C., Jackson, A., Lammers, L. N., Torchinsky, A. B., Weaver, K. L., Bird, D. K., and Brown, G. E.: A spatially resolved surface kinetic model for forsterite dissolution, Geochim Cosmochim Ac, 174, 313-334, 10.1016/j.gca.2015.11.019, 2016.

Moosdorf, N., Renforth, P., and Hartmann, J.: Carbon dioxide efficiency of terrestrial enhanced weathering, Environ Sci Technol, 48, 4809-4816, 10.1021/es4052022, 2014.